162

JOURNAL OF MAGNETIC RESONANCE **96,** 432–440 (1992)

Improved 3D Triple-Resonance NMR Techniques Applied to a 31 kDa Protein

STEPHAN GRZESIEK* AND AD BAX

Laboratory of Chemical Physics, National Institute of Diabetes and Digestive and Kidney Diseases, National Institutes of Health, Bethesda, Maryland 20892

Received September 6, 1991

Recently proposed 3D triple-resonance techniques (*1–5*) make it possible to obtain sequential assignment of the backbone ^{1}H, ^{15}N, and ^{13}C resonances in proteins that can be isotopically labeled with ^{13}C and ^{15}N. This approach has been used successfully for a number of systems, including calmodulin (16.7 kDa) (*1*), calmodulin complexed with a 26-residue peptide (~20 kDa) (*6*), and the phospho-carrier protein III^{Glc} (*7*) (18 kDa). All of these triple-resonance experiments rely on transfer of magnetization via heteronuclear one-bond J couplings and the sensitivity of the experiments depends strongly on the ratio of the size of the J coupling and the linewidths of the nuclei involved in the magnetization transfer process. Our original experiments were designed to minimize the number of RF pulses required for a particular pulse sequence, and thus to minimize the effect of pulse imperfections. Subsequent experience with these experiments has indicated that the effect of pulse imperfections is not as severe as originally expected, provided that pulses are properly calibrated. Hence, in order to optimize the experiments it is more important to minimize the relaxation of transverse magnetization by keeping the dephasing and rephasing delays as short as possible, especially for larger proteins. Here we demonstrate the applicability of three improved triple-resonance experiments to the study of interferon-γ, a dimer with 134 residues per monomer and a total molecular weight of 31.4 kDa.

Correlation of the amide proton and ^{15}N resonance with the intraresidue $^{13}C\alpha$ can be obtained with an experiment known as HNCA (*1, 2*). Note that this experiment also provides connectivity to the Cα of the preceding residue, transferring coherence via the $^{2}J_{N-C\alpha}$ coupling. Because $^{1}J_{N-C\alpha}$ and $^{2}J_{N-C\alpha}$ can be of comparable magnitude (*8*) it may not always be possible to distinguish intra- from interresidue connectivities with this experiment. In contrast, the HN(CO)CA experiment (*4*) provides correlations exclusively to the Cα resonance of the preceding residue by relaying magnetization via the intervening carbonyl ^{13}C spin. The HN(CO)CA experiment is closely related to the HNCO experiment, which correlates the amide ^{1}H and ^{15}N with the ^{13}C of the preceding residue. In the present study of interferon-γ, we employ modified versions of these experiments, using INEPT (*9*) instead of HMQC (*10–12*) type coherence transfers, and overlay the ^{13}C–^{15}N dephasing period with a ^{15}N evolution period

* On leave from F. Hoffmann–LaRoche Ltd., Basel, Switzerland.

0022-2364/92 $3.00

of the "constant-time" variety (*5, 13–15*). Advantages of these modifications are discussed below.

The pulse schemes for the modified experiments are shown in Fig. 1. The third experiment, CT-HN(CO)CA (Fig. 1c), differs from the original version (*4*) only by the use of a constant-time t_1 evolution period in the present experiment. This eliminates decay of magnetization that normally occurs during the t_1 evolution period and it permits the use of linear prediction with "mirror image constraint" (*16*) since the signal in the t_1 dimension is a sum of undamped cosinusoidal oscillations of known phase (0°). A detailed description of the magnetization-transfer steps of the HN(CO)CA experiment was presented previously (*4*) and will not be repeated here. The new pulse schemes for the CT-HNCA and CT-HNCO experiments are more similar to those of the CT-HN(CO)CA experiment than to the original HNCA and HNCO sequences (*2*). The CT-HNCO and CT-HNCA schemes differ from one another only by the interchanged ^{13}CO and ^{13}Cα channels and a different choice of delay durations. Therefore, in the following discussion of the magnetization transfer during the pulse sequences we restrict ourselves to the CT-HNCA experiment.

For the CT-HNCA experiment, the relevant magnetization-transfer steps are outlined using the product-operator formalism. For clarity, relaxation terms are not included and constant multiplicative factors are omitted. Only terms that result in observable magnetization during the detection period, t_3, are retained. The spin operators used are I for the amide proton, N for the amide ^{15}N, S for the carbonyl ^{13}C, and A_1 and A_2 for the intraresidue Cα and for the Cα of the preceding residue, respectively. J_{XY} denotes the J coupling between spins X and Y and RF phases correspond to the first step of the phase cycle given in the legend to Fig. 1.

Longitudinal amide proton magnetization (I_z), present at the start of the experiment, is converted into antiphase ^{15}N magnetization by an INEPT type transfer. Thus, at time a in Fig. 1a the spin system is described by $\sigma_a = N_y I_z \sin(2\pi J_{NH}\tau)$. Evolution due to J coupling during the subsequent constant-time evolution period (of total duration $2T$) is independent of the duration of t_1, but ^{15}N chemical-shift evolution depends on t_1 in the regular manner. The constant time is set to an integral multiple of $1/J_{NH}$ (22 ms in the present case), such that at time b the ^{15}N magnetization has remained antiphase with respect to its attached proton spin. Ignoring the $\sin(2\pi J_{NH}\tau)$ term present at time a, the magnetization at time b is described by

$$\sigma_b = N_x I_z A_{1z} \sin(2\pi J_{A_1N}T)\cos(2\pi J_{A_2N}T)\cos(\Omega_N t_1) + N_x I_z A_{2z} \sin(2\pi J_{A_2N}T)\cos(2\pi J_{A_1N}T)\cos(\Omega_N t_1), \quad [1]$$

where Ω_N denotes the angular offset frequency of the ^{15}N spin. This magnetization is transferred into antiphase Cα magnetization by the $90^\circ_{\phi 6}$ and $90^\circ_{\phi 7}$ pulses, yielding at time c

$$\sigma_c = A_{1y} N_z I_z + A_{2y} N_z I_z, \quad [2]$$

where the trigonometric terms of expression [1] again have been omitted temporarily. At the end of the t_2 evolution period, the terms that will be transferred back into observable magnetization are represented by

$$\sigma_d = A_{1y} N_z I_z \cos(\Omega_{A_1} t_2) + A_{2y} N_z I_z \cos(\Omega_{A_2} t_2). \quad [3]$$

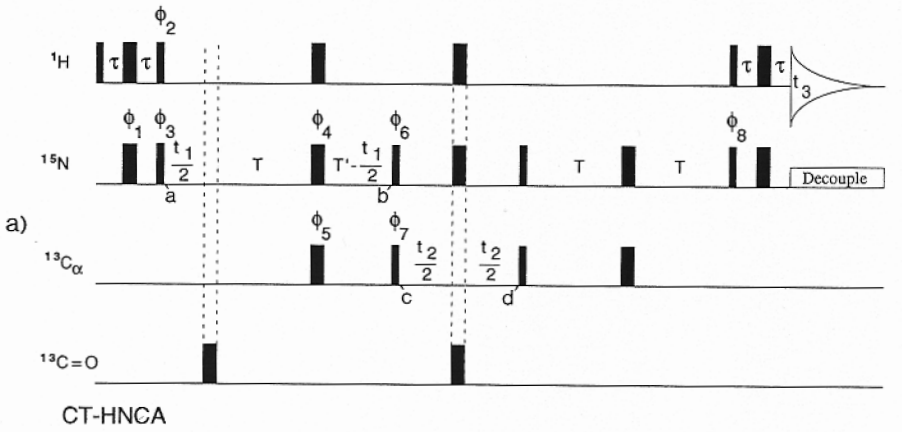

CT-HNCA

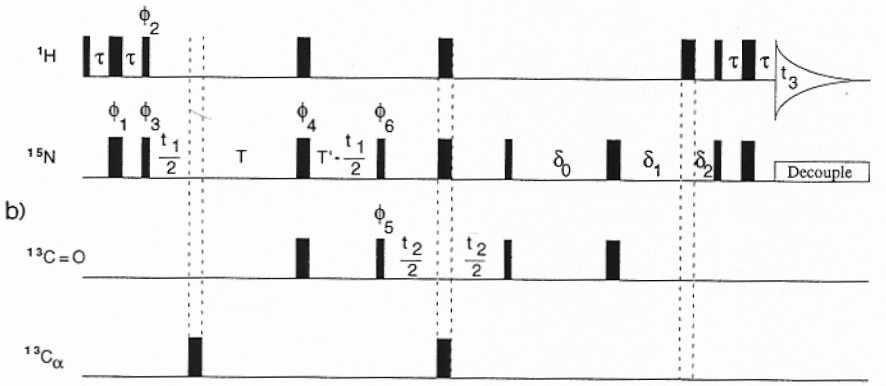

CT-HNCO

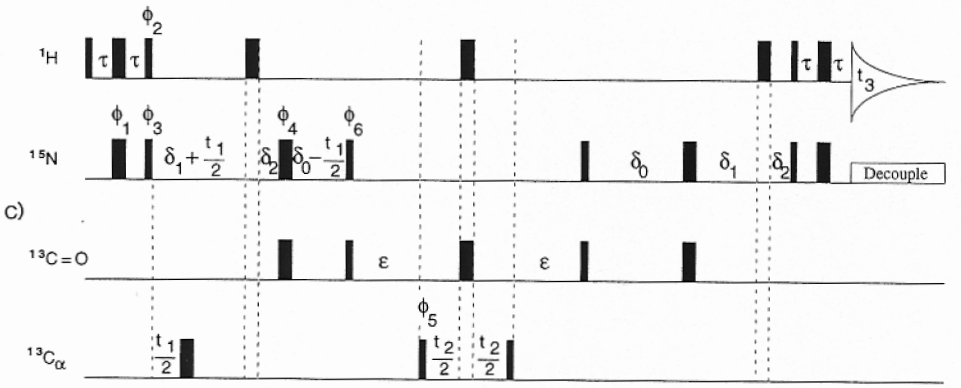

CT-HN(CO)CA

Transfer of this magnetization back into observable amide proton magnetization follows the reverse pathway of that described above. At the beginning of the detection period, the observable magnetization is described by

$$\sigma_e = \sin^2(2\pi J_{NH}\tau)\cos(\Omega_N t_1) I_x[\sin^2(2\pi J_{A_2N}T)\cos^2(2\pi J_{A_1N}T)\cos(\Omega_{A_2}t_2) + \sin^2(2\pi J_{A_1N}T)\cos^2(2\pi J_{A_2N}T)\cos(\Omega_{A_1}t_2)], \quad [4]$$

where all relevant trigonometric terms have been reintroduced. This expression is identical to that derived for the original HNCA experiment (eq. [4] in Ref. (*2*)). The difference between the constant-time and the original experiment is found in the relaxation terms which have been neglected in the discussions of both experiments. Because in the present experiment signal does not decay as t_1 increases, a substantial gain in sensitivity can be obtained. This again, G, is given approximately by

$$G = AT_1 \Big/ \int_0^{AT_1} \exp(-t_1/T_{2N})dt_1, \quad [5]$$

where AT_1 is the duration of the t_1 acquisition time and T_{2N} is the ^{15}N T_2 value in the ^1H-coupled mode. For the present study of interferon-γ, T_{2N} equals approximately 24 ms, and $AT_1 = 22$ ms, yielding a gain, G, in signal-to-noise of 1.5. A further gain in sensitivity can be obtained if the pulse schemes are modified to utilize composite-pulse ^1H decoupling instead of 180° pulses, as indicated in Fig. 2. As shown previously (*17*) the ^{15}N transverse relaxation rate becomes approximately 30% slower in this case since the ^{15}N transverse magnetization remains in-phase with respect to its attached ^1H. This increase in the apparent T_{2N} reduces the signal loss caused by ^{15}N transverse relaxation during the delays of total duration $4T$. Because of the limited stability of interferon-γ and the small amount of available sample, we have been unable to test and compare the schemes of Fig. 2 with the results obtained with the schemes of Fig. 1. However, when the experimental results obtained for the protein calmodulin (16.7 kDa) are compared, a gain of a factor 1.2 is observed with the schemes of Fig. 2 over the schemes of Fig. 1. For interferon-γ, which has a much faster rate of ^1H spin diffusion, this gain is expected to be $\sim$1.5.

In the present experiment, the signal decay in the t_2 dimension is determined by the $^{13}C\alpha$ transverse relaxation time, whereas in the original HNCA experiment it was

---

FIG. 1. Pulse sequences of the (a) CT-HNCA, (b) CT-HNCO, and (C) CT-HN(CO)CA experiments. Narrow pulses correspond to a 90° flip angle and wide pulses to 180°. Pulses for which the RF phase is not marked are applied along the x axis. The power and duration of Cα pulses are adjusted such that they have a null in their excitation profile at the ^{13}CO frequency, and vice versa. Delay duration for the three pulse schemes are $\tau = 2.25$ ms; $T = 13.5$ ms; $T' = T + \tau_{180°}(^{13}C)$, where $\tau_{180°}(^{13}C)$ is the 180° (CO) pulse width (162 μs) for scheme (a) and the 180° (Cα) pulse width (108 μs) for scheme (b); $\delta_1 = 7.25$ ms; $\delta_2 = 2.75$ ms; $\delta_0 = \delta_1 + \delta_2 + \tau_{180°}(^1H)$; $\epsilon = 6$ ms. The phase cycling used is as follows. For scheme (a), $\phi_1 = x, -x$; $\phi_2 = y, -y$; $\phi_3 = x$; $\phi_4 = 4(x), 4(y), 4(-x), 4(-y)$; $\phi_5 = 16(x), 16(-x)$; $\phi_6 = 16(y), 16(-y)$; $\phi_7 = x, x, -x, -x$; $\phi_8 = y$; Acq. $= 2(x, -x, -x, x, -x, x, x, -x), 2(-x, x, x, -x, x, -x, -x, x)$. For schemes (b) and (c), $\phi_1 = x, -x$; $\phi_2 = y, -y$; $\phi_3 = x$; $\phi_4 = 4(x), 4(y), 4(-x), 4(-y)$; $\phi_5 = x, x, -x, -x$; $\phi_6 = x, -x$; Acq. $= 2(x), 4(-x), 2(x)$. For scheme (a), quadrature in the t_1 and t_2 dimensions is accomplished by altering the phases ϕ_3 and ϕ_7 in a States–TPPI manner (*20*). For schemes (b) and (c), the phases of ϕ_3 and ϕ_5 must be altered in a States–TPPI manner to obtain quadrature in these two dimensions.

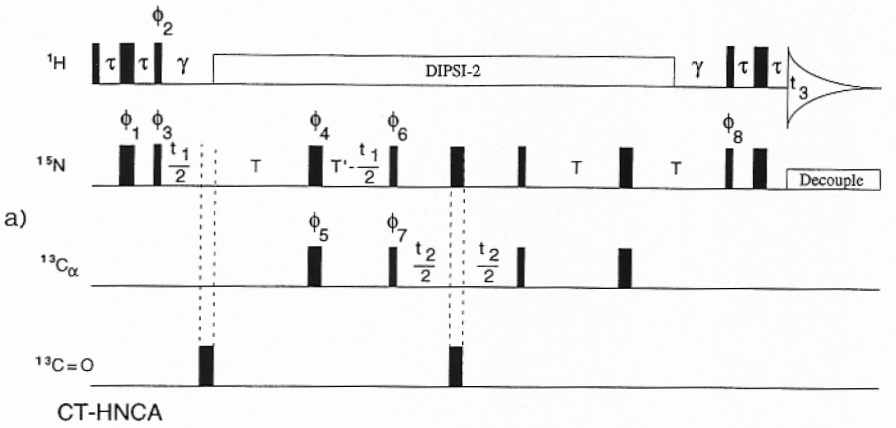
a)
CT-HNCA
DIPSI-2
Decouple

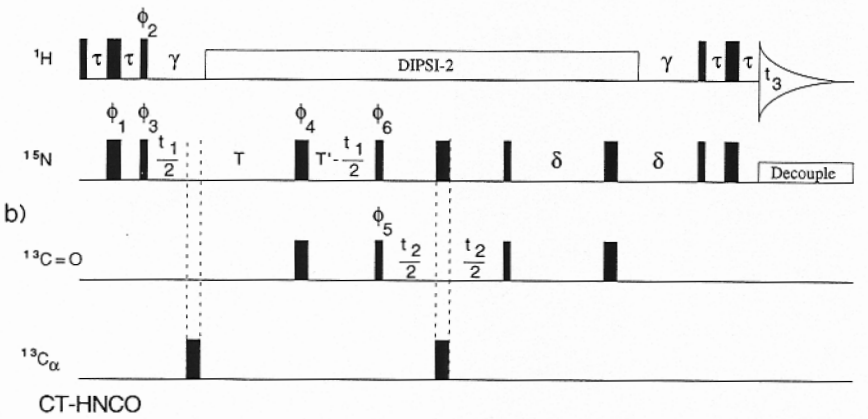
b)
CT-HNCO
DIPSI-2
Decouple

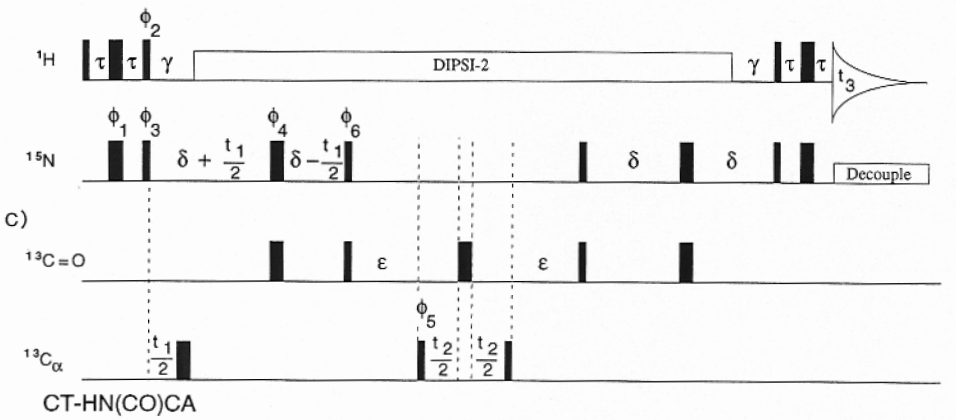
c)
CT-HN(CO)CA
DIPSI-2
Decouple

determined by the decay rate of three-spin (I, N, and A) coherence. In both cases, however, the resolution is limited by the fact that the Cα resonance is coupled to ^{13}Cβ and it is generally undesirable to resolve this J splitting. Therefore, the acquisition time in the t_2 dimension is kept shorter than $1/(2J_{C\alpha C\beta})$, about 10 ms in practice, and the difference in intrinsic relaxation rates of transverse ^{13}Cα magnetization and three-spin coherence is of no practical consequence.

The constant-time version of the HNCO experiment, shown in Fig. 1b, is essentially the same as the CT-HNCA scheme of Fig. 1a. Note, however, that a slightly longer constant-time acquisition period can be used in this experiment because, in contrast to the HNCA case, ^{15}N dephases only under the influence of coupling to a single ^{13}C spin. The time $2T$ is now set to an odd multiple of $1/(2J_{NH})$ (27 ms in our case), such that the magnetization is in-phase with respect to the amide proton spin (N_yS_z) when it is transferred to the ^{13}C spin. This is important because for t_2 acquisition times shorter than ~50 ms (i.e., before significant antiphase magnetization develops) this lengthens the apparent relaxation time of the ^{13}CO spin (which only has small long-range J couplings to other protons). If the ^{13}CO magnetization were antiphase with respect to the amide proton spin its decay rate would increase by the rate of ^{1}H–^{1}H spin flips. The comparable scheme of Fig. 2b provides the same initial decay rate in the t_2 dimension as the scheme of Fig. 1b, but is expected to yield superior ^{13}CO resolution if acquisition times much longer than 50 ms are used in the t_2 dimension. In addition, magnetization loss caused by ^{15}N relaxation during the intervals $2T$ and δ_0 and δ_1 is reduced in the scheme of Fig. 2b for reasons mentioned above. Note that in the original HNCO experiment (*2*), the ^{13}CO frequency was obtained from an HMQC type correlation with ^{15}N, and in that case, dephasing in the t_2 dimension caused by $^1J_{C\alpha N}$ and $^2J_{C\alpha N}$ limits the obtainable resolution.

The pulse schemes shown in Fig. 1 are demonstrated for the protein interferon-γ, a homodimer with 134 residues per monomer and a total molecular weight of 31.4 kDa. The protein was labeled uniformly with ^{13}C (>95%) and ^{15}N (~50%) and purified according to the procedure described by Doebeli *et al.* (*18*). Experiments were conducted on a sample containing 0.7 mM dimer in 95%/5% H_2O/D_2O, pH 6.3, 27°C, using an unmodified Bruker AMX-600 spectrometer.

Figure 3 shows three cross sections of the three different types of 3D spectra. All are taken perpendicular to the ^{15}N axis at a ^{15}N frequency of 119 ppm. The position of these slices in the ^{1}H–^{15}N shift correlation spectrum is indicated by a dotted line

---

FIG. 2. Alternative versions of the pulse schemes shown in Fig. 1, using composite-pulse decoupling to remove J coupling between protons and ^{15}N/^{13}C. The delay γ is set to $1/(2J_{NH})$: the phase cycling and all other durations are identical to those given in the legend to Fig. 1, except for ϕ_6 of schemes (b) and (c) which is given by $\phi_6 = y, -y$ and $\delta = 10$ ms. To minimize the effect of ^{15}N transverse magnetization decay caused by homonuclear J coupling, a decoupling scheme of the DIPSI type (*21*) is preferred. Note that the 90° and 180° pulses applied to the heteronucleus to which the proton is coupled interfere destructively with composite pulse decoupling and a higher power level is needed for the ^{1}H decoupling compared to the normal case in which decoupling is used while observing the second nucleus. For a ^{1}H RF field strength stronger than ~4 kHz this effect is not noticeable. For reproducible water suppression it is necessary to perform the DIPSI decoupling in a synchronous mode, i.e., to start the decoupling at the same position during the decoupling cycle each time it is used.

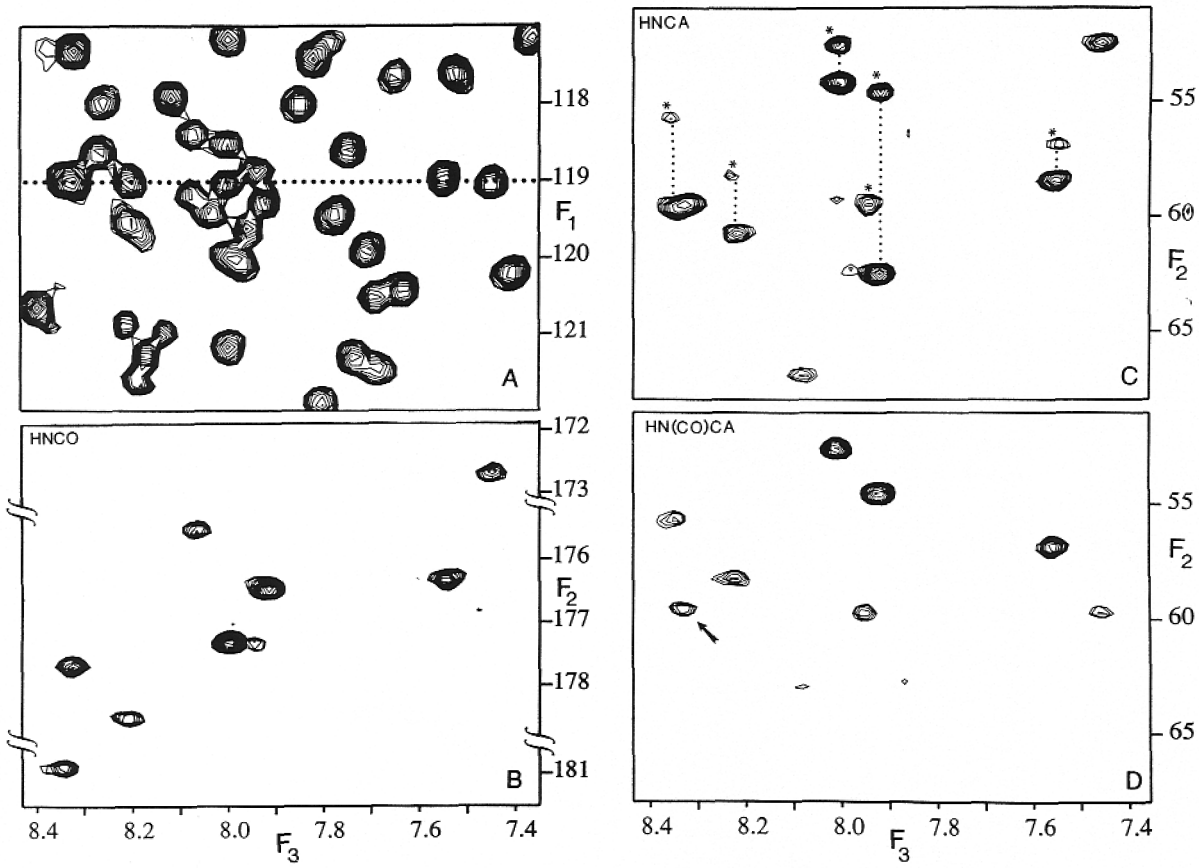

FIG. 3. Spectra obtained for a sample of interferon-γ (8.8 mg in 0.4 ml H_2O/D_2O), labeled uniformly with ^{13}C (>95%) and ^{15}N (50%). (A) Small region of the resolution-enhanced 2D Overbodenhausen (HSQC) spectrum. The dotted line marks the position where the slices through the 3D spectra are taken. (B) F_1 = 119 ppm slice of the CT-HNCO spectrum, recorded with the pulse sequence of Fig. 1b. (C) F_1 = 119 ppm slice of the CT-HNCA spectrum, recorded with the pulse sequence of Fig. 1a. (D) F_1 = 119 ppm slice of the CT-HN(CO)CA spectrum, recorded with the pulse sequence of Fig. 1c. All 3D spectra have been processed using linear prediction with mirror image constraint in the F_1 dimension. The CT-HNCA spectrum results from a (32 complex) × (48 complex) × (512 complex) data matrix with 256 scans per hypercomplex (t_1, t_2) increment, and acquisition times of 22.4, 10.0, and 55.3 ms in the t_1, t_2, and t_3 dimension, respectively. The CT-HNCO spectrum results from a (32 complex) × (64 complex) × (512 complex) data matrix with 64 scans per hypercomplex (t_1, t_2) increment, and acquisition times of 24.0, 34.5, and 55.3 ms in the t_1, t_2, and t_3 dimension, respectively. The CT-HN(CO)CA spectrum results from a (32 complex) × (46 complex) × (512 complex) data matrix with 128 scans per hypercomplex (t_1, t_2) increment, and acquisition times of 19.8, 9.6, and 55.3 ms in the t_1, t_2, and t_3 dimension, respectively.

in the 2D ^1H–^{15}N correlation spectrum of Fig. 3A. Because the linewidth in the F_1 (^{15}N) dimension of the 3D spectrum is approximately double the ^{15}N linewidth in the 2D spectrum, resonances in Fig. 3A that are close to the dotted line, with their ^{15}N chemical shift differing by less than 0.2 ppm from 119.0 ppm, also give rise to resonances in the (F_1 = 119 ppm) slice shown for each of the 3D spectra.

The HNCO spectrum of which the F_1 = 119 ppm slice is shown in Fig. 3B clearly has the highest signal-to-noise ratio of the three 3D spectra. This was expected since the ^{15}N–^{13}CO coupling is larger than the ^{15}N–$^{13}C\alpha$ J coupling, making transfer more efficient than in the HNCA experiment. Note that resonance intensity in the HNCA spectrum (Fig. 3C) is also lowered because the ^{15}N–$^{13}C\alpha$ transfer is attenuated by the presence of the additional passive ^{15}N–$^{13}C\alpha$ J coupling (cf. Eq. [4]). Nevertheless, in the HNCA spectrum of Fig. 3C both intra- and interresidue HN–N–Cα correlations are observed for the majority of the amides. The interresidue connectivities in Fig. 3C are distinguished from the intraresidue ones by comparison with the HN(CO)CA spectrum of Fig. 3D. A recent low-resolution X-ray study (*19*) indicates that interferon-γ is largely α-helical and contains no β-sheet. Two-bond ^{15}N–$^{13}C\alpha$ J couplings in α-helices (6.4 ± 0.4 Hz) are significantly smaller than those in β-sheets (8.4 ± 0.5 Hz) (*8*), and it is therefore remarkable that these connectivities are observable despite the fact that the ^{15}N linewidths are approximately twice the size of this coupling, and despite the fact that the protein accidentally was labeled at a level of only 50% with ^{15}N. Figure 3D has been acquired with the HN(CO)CA technique, which contains an extra relay step compared to the HNCA and HNCO methods. However, because the relay of magnetization via the ^{13}CO nucleus is quite efficient, sensitivity of the 3D spectrum is high. A number of additional interresidue connectivities are observed relative to the spectrum of Fig. 3C, and an interresidue correlation that was obscured by overlap with the intraresidue correlation in the HNCA spectrum is clearly observed in Fig. 3D and marked with an arrow.

Before the backbone assignment of interferon-γ can be completed, it is necessary to get residue type assignments for at least a significant fraction (>10%) of the amides. To this extent, preparation of more uniformly labeled sample, needed because of its limited stability, is currently in progress. The present report clearly indicates, however, that the triple-resonance assignment procedure outlined previously (*1*) is applicable to proteins of a molecular weight larger than anticipated. It is noteworthy that the present study was carried out at a relatively low temperature (27°C), and that after correcting for the low level of ^{15}N labeling, the effective protein monomer concentration was only 0.7 mM. Of course, the spectral complexity for a symmetric dimer such as interferon-γ is much lower than that for a regular protein of the same molecular mass. However, in the present 3D spectra, resonance overlap is rather minimal and a doubling of the total number of correlations is not expected to cause unsurmountable problems.

ACKNOWLEDGMENTS

We thank Drs. R. Gentz and H. Doebeli for the expression and purification of the labeled interferon-γ, Dr. W. Vetter and W. Meister for analytical mass spectroscopy, Dr. M. Zulauf for quasi-electric light scattering analysis, Dr. W. Klaus for the initial NMR characterization, and Dr. A. M. Labhardt for his enthusiastic support. S.G. acknowledges funding by the ROCHE Research Foundation. This work was supported by the Intramural AIDS targeted Anti-Viral Program of the Office of the Director of the National Institutes of Health.

REFERENCES

1. M. IKURA, L. E. KAY, AND A. BAX, *Biochemistry* **29,** 4659 (1990).
2. L. E. KAY, M. IKURA, R. TSCHUDIN, AND A. BAX, *J. Magn. Reson.* **89,** 496 (1990).
3. L. E. KAY, M. IKURA, AND A. BAX, *J. Magn. Reson.* **91,** 84 (1991).

4. A. BAX AND M. IKURA, *J. Biomol. NMR* **1,** 99 (1991).
5. R. POWERS, A. M. GRONENBORN, G. M. CLORE, AND A. BAX, *J. Magn. Reson.* **94,** 209 (1991).
6. M. IKURA, L. E. KAY, M. KRINKS, AND A. BAX, *Biochemistry* **30,** 5498 (1991).
7. J. G. PELTON, D. A. TORCHIA, N. D. MEADOW, C.-Y. WONG, AND S. ROSEMAN, *Biochemistry* **30,** 10,043 (1991).
8. F. DELAGLIO, D. A. TORCHIA, AND A. BAX, *J. Biomol. NMR,* in press.
9. G. A. MORRIS AND R. FREEMAN, *J. Am. Chem. Soc.* **101,** 760 (1979).
10. L. MUELLER, *J. Am. Chem. Soc.* **101,** 4481 (1979).
11. M. R. BENDALL, D. T. PEGG, AND D. M. DODDRELL, *J. Magn. Reson.* **52,** 81 (1983).
12. A. BAX, R. H. GRIFFEY, AND B. L. HAWKINS, *J. Magn. Reson.* **55,** 301 (1983).
13. A. BAX, A. F. MEHLKOPF, AND J. SMIDT, *J. Magn. Reson.* **35,** 373 (1979).
14. A. BAX AND R. FREEMAN, *J. Magn. Reson.* **44,** 542 (1981).
15. O. W. SØRENSEN, *J. Magn. Reson.* **90,** 433 (1990).
16. G. ZHU AND A. BAX, *J. Magn. Reson.* **90,** 405 (1990).
17. A. BAX, M. IKURA, L. E. KAY, D. A. TORCHIA, AND R. TSCHUDIN, *J. Magn. Reson.* **86,** 304 (1990).
18. H. DOEBELI, R. GENTZ, W. JUCKER, G. GAROTTA, D. W. HARTMANN, AND E. HOCHULI, *J. Biotechnol.* 7, 199 (1988).
19. S. E. EALICK, W. J. COOK, S. VIJAY-KUMAR, M. CARSON, T. L. NAGABHUSHAN, P. P. TROTTA, AND C. E. BUGG, *Science* **252,** 698 (1991).
20. D. MARION, M. IKURA, R. TSCHUDIN, AND A. BAX, *J. Magn. Reson.* **85,** 393 (1989).
21. A. J. SHAKA, C. J. LEE, AND A. PINES, *J. Magn. Reson.* **77,** 274 (1988).